RSC Advances

ROYAL SOCIETY OF CHEMISTRY

www.rsc.org/advances

RSCPublishing

ARTICLE

Design and Tailoring of Three-dimensional Graphene–Vulcan carbon–Bi_2S_3 Ternary Nanostructures for High-Performance Lithium-Ion-Battery Anodes

Cite this: DOI: 10.1039/x0xx00000x

Received 00th January 2012,
Accepted 00th January 2012

DOI: 10.1039/x0xx00000x

www.rsc.org/

Seung-Keun Park,[a,b] Seunghee Woo,[c] Sohee Lee,[a] Chae-Yong Seong,[a]

Yuanzhe Piao*[a,b]

Design of the structure and morphology of electrode materials is crucial for creating short transport pathways of lithium ions and electrons in high-performance lithium-ion battery systems. Here, a strategy for preparing three-dimensional (3D) carbon-based architectures consisting of bismuth sulfide (Bi_2S_3) and Vulcan carbon spheres intercalated between graphene sheets is proposed. Bi_2S_3 nanoparticles were successfully deposited on the graphene/Vulcan carbon composite via a facile ultrasonic route, followed by a thermal treatment process for achieving high crystallinity. In the unique hybrid structure, commercial Vulcan carbon, a low-priced and mass produced carbon material, acts as a nanospacer, thereby preventing the restacking of graphene nanosheets and thus increasing the surface area of the composite. In addition, it also provides an additional electron-transport pathway, increasing the electrolyte/electrode interface contact and facilitating transport of the electron and lithium ions into the bulk of the composite. Consequently, the 3D graphene–Vulcan carbon–Bi_2S_3 nanocomposite exhibited a high reversible capacity of 702 mA h g^{-1} (graphene/Vulcan = 3:1 wt%) after 100 cycles and excellent rate performance compared of graphene–Bi_2S_3 nanocomposites, demonstrating the potential of 3D graphene–Vulcan carbon–Bi_2S_3 nanocomposites for use as the anode material for lithium-ion batteries.

1. Introduction

During the past decades, various energy storage systems have played an increasingly important role in our life. Among the currently available energy storage systems, Li-ion battery (LIB) has received considerable attention because of its affordability, high energy density, and environmental benignity.[1, 2] To achieve higher power and energy density, it is necessary to explore advanced electrode materials with higher capacity levels compared to those currently used. Therefore, many studies have focused on replacing the commonly used graphite anode with electrodes of metal oxides or sulfides, which afford a high capacity of 600–1000 mA h g^{-1}.[3-8]

Some metal sulfides such as MoS_2, FeS_x, and Bi_2S_3 have emerged as anode or cathode materials for LIBs because of their high specific capacity.[9-12] Among them, bismuth sulfide (Bi_2S_3), which is a metal chalcogenide, is an interesting anode material for LIBs because of its high stability and theoretical capacity of 625 mA h g^{-1}. However, most bismuth sulfides show low electrical conductivity and high volume expansion during cycling, resulting in a fast capacity fading within few cycles. These drawbacks limit their application in LIBs. Therefore, various proposals have been presented to improve their electrochemical properties. One of most effective ways is to use carbonaceous materials that can act as a buffer matrix against volume expansion during cycling and as a conductive substrate.[13, 14]

Recently, graphene, a two-dimensional carbon material with sp^2 bonding, has been considered as a new matrix material to improve electrochemical performance of bismuth sulfides. For example, Zhang et al. synthesized Bi_2S_3@graphene nanocomposites by a hydrothermal method and reported that the Bi_2S_3@graphene electrodes exhibit a high capacity of 400.5 mA h g^{-1} after 50 cycles at a current density of 100 mA g^{-1} with 95% capacity retention.[15] However, the poor electrical contacts between the reduced graphene oxide (rGO) sheets lower the electrode conductivity of the graphene-based composites. In addition, during the reduction process, the formation of irreversible rGO agglomerates by π-π interaction results in the decrease of overall surface area of the composites.[16, 17] Because of the aggregation of rGO sheets, the outstanding performance of graphene-based composites is significantly lost, which is one of the most important issues for using graphene-based composites in electrode materials. One possible approach to manage the problems mentioned above is to use physical spacers to retain the high surface area of graphene.[18-21] In previous reports, carbon nanotubes (CNTs) or mesoporous carbon is used as physical spacers, but they are expensive and have complex synthesis procedures.[22-25]

Herein, we demonstrate a facile sonochemical method to synthesize a three-dimensional (3D) graphene–Vulcan carbon–Bi_2S_3 nanocomposite, in which the small Bi_2S_3 nanoparticles are grown on graphene and Vulcan carbon. Commercial Vulcan carbon, a cheap

and mass produced carbon source, not only reduces the contact resistance between graphene sheets acting as bridge but can also act as a physical spacer to inhibit the restacking of graphene sheets, resulting in a high surface area, to enhance electrolyte accessibility and facilitating transportation of the Li ions and electrons into the bulk of the electrode. As a consequence, the 3D graphene–Vulcan carbon–Bi_2S_3 nanocomposites exhibit higher reversible capacities than that of Bi_2S_3–graphene nanocomposites, and significantly enhanced cycling and rate performances.

2. Experimental

Synthesis of 3D graphene–Vulcan carbon–Bi_2S_3 composites

Bi_2S_3 nanoparticles deposited on graphene–Vulcan carbon composites were prepared using a two-step method: hydrolysis of $Bi(NO_3)_3{\cdot}5H_2O$ in the presence of graphene oxide (GO), Vulcan carbon, and thioacetamide (TAA), followed by heating at 200°C. GO was prepared by a modified Hummers method.[26] Typically, GO (90 mg) and Vulcan carbon (30 mg, weight ratio 3:1) were dispersed in an aqueous TAA solution (0.15 g, 90 ml). To this solution, $Bi(NO_3)_3{\cdot}5H_2O$ (0.485 g) dispersed in DI water (10 ml) was added slowly using a pipette, and the mixture was further agitated by sonication for 1 h. After the reaction, the solid precipitate was filtered and washed repeatedly with DI water and ethanol. To improve crystallinity and reduce GO, the obtained powder was heated at 200°C for 2 h under an inert atmosphere. The obtained composite with 3:1 weight ratio of GO/Vulcan carbon was designated as GVB (3:1). The graphene–Bi_2S_3 (GB) and bare Bi_2S_3 samples were also prepared via the same procedures without using Vulcan carbon and graphene–Vulcan carbon, respectively. In order to investigate the effects of GO/Vulcan carbon weight ratio on the electrochemical properties, composites with 1:1 and 1:3 weight ratios of GO to Vulcan carbon were prepared in the same way as GVB (3:1) and designated as GVB (1:1) and GVB (1:3), respectively.

Material Characterization

Crystallographic information about GVB and Bi_2S_3 nanorod samples was investigated using X-Ray diffraction (XRD using a D8-advance, equipped with a Cu Kα radiation source (λ = 1.5406 Å)). The structures and morphologies of all samples were identified by field emission scanning electron microscopy (FE-SEM, Hitachi S-4800). A JEM-2010 transmission electron microscope (TEM) equipped with an energy-dispersive X-ray spectrometer (EDX) was operated at 200 kV to obtain high-resolution TEM measurements. For thermo gravimetric analysis (TGA), a Mettler Toledo TGA/DSC 1 model was used with a heating rate of 10°C min^{-1} in air. Nitrogen adsorption and desorption isotherms were measured on a BELSORP-mini II (BEL Japan).

Electrochemical measurements

To evaluate the electrochemical properties of samples, a slurry composed of 70 wt% active materials, 20 wt% Super-P as a conductive carbon, and 10 wt% polyvinylidenefluoride (PVDF) in *n*-methyl-2-pyrrolidone was coated on a copper foil. After drying, coin-type cells (2016 type) were assembled in an argon-filled glove box. Li metal was used as both counter and reference electrodes and the electrolyte was 1.0 M $LiPF_6$ dissolved in a 1:1 mixture (by volume) of ethylene carbonate (EC) and diethyl carbonate (DEC). Galvanostatic charge/discharge tests were performed on a WBCS3000s cycler (WonATech, Korea) using a voltage window of 0.01 and 3.0 V vs. Li/Li^+. In term of capacity of the GVB composites, all samples are based on the total weight of the composites.

3. Results & discussion

Fig. 1a and b show the XRD patterns of the bare Bi_2S_3 rods and GVB (3:1), respectively. All the diffraction peaks in both patterns can be clearly indexed to the Bi_2S_3 phase with the space group, P*bnm* (PDF#17-0320).[27] In the XRD pattern of GVB (3:1), the absence of peaks related to Vulcan carbon and graphene can be attributed to the low intensity compared to Bi_2S_3 nanoparticles and overlap with a peak related to the (130) lattice plane of Bi_2S_3 nanoparticles. In addition, all the peaks of GVB (3:1) are broader than that of bare Bi_2S_3 nanorods, implying a small particle size of Bi_2S_3.

TGA was used to confirm the amount of Bi_2S_3 and carbon in GB and GVB nanocomposites. A weight loss of 1.5 wt% below 100°C is because of the dissipation of the adsorbed water on the samples. The TGA curves of the samples exhibit a variation in weight between 300 and 490°C, which may be attributed to the oxidation of bismuth sulfides, when the sulfur species may be lost as sulfur dioxide (SO_2)

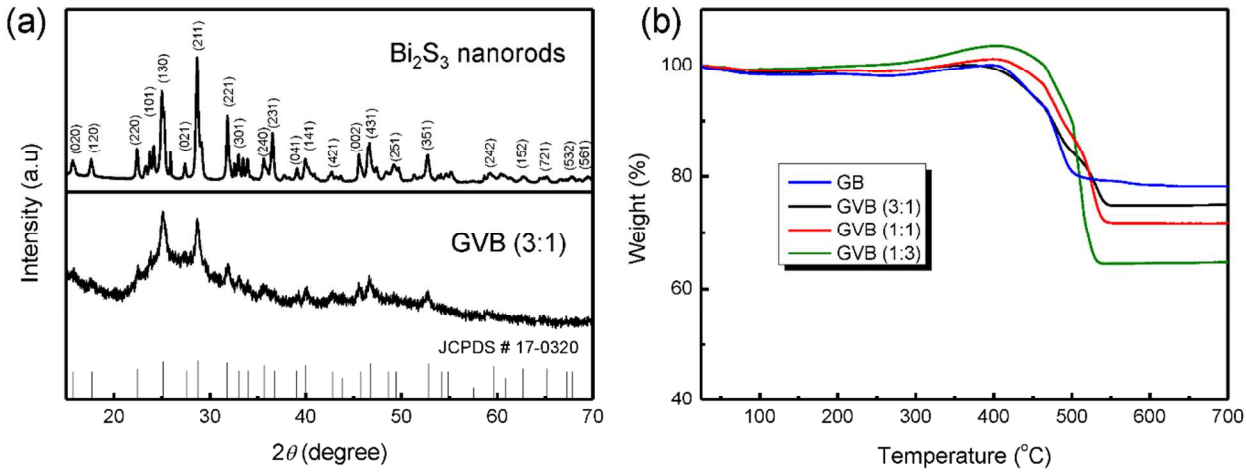

Fig. 1 (a) XRD patterns of Bi_2S_3 nanorods and GVB (3:1), (b) TGA curves of GV, GVB (3:1), GVB (1:1), and GVB (1:3)

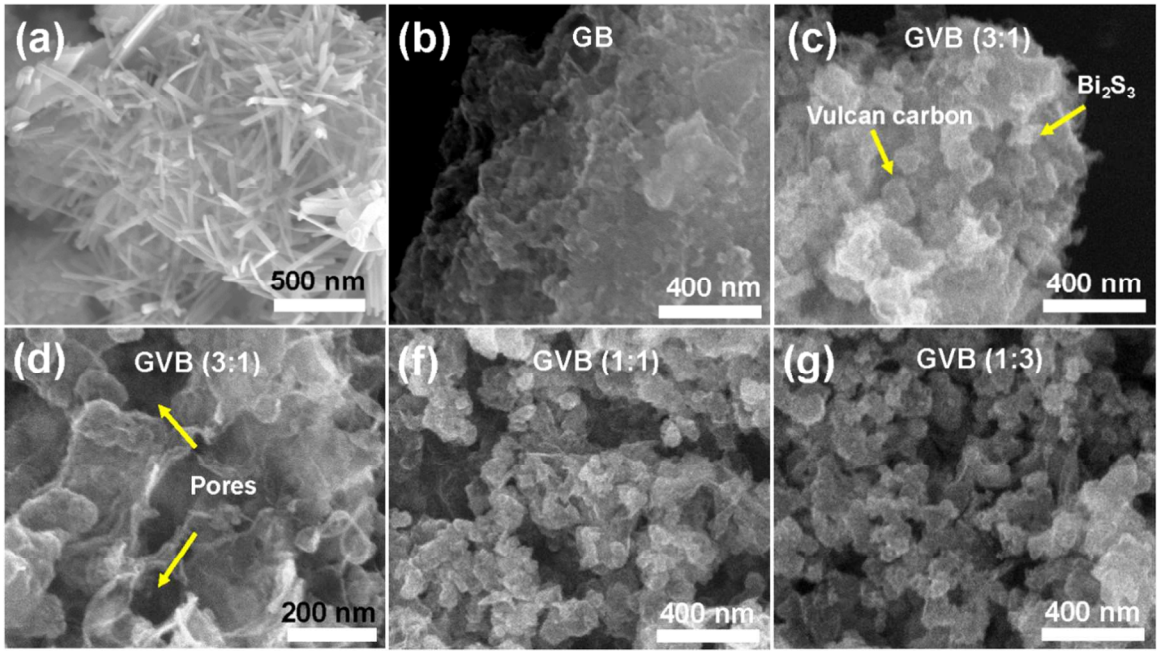

Fig. 2 SEM images of (a) Bi_2S_3 nanorods, (b) GB, and (c–g) 3D GVB nanocomposites

gas or deposited as the sulfate (SO_4^{2-}) species.[14] The weight loss is caused by the combustion of carbonaceous materials. Therefore, the loading mass of Bi_2S_3 in GB, GVB (3:1), GVB (1:1), and GVB (1:3) is calculated to be 78.3, 75, 71, and 64 wt%, respectively. Interestingly, the amount of Bi_2S_3 increased with the increasing GO content in composites, which may be attributed to the interaction between the oxygen-containing groups on the surface of GO and bismuth metal ion.

Morphologies of the Bi_2S_3, GB, and GVB nanocomposites observed by SEM are shown in Fig. 2. In the absence of GO, a rod-shaped Bi_2S_3 with a diameter of about 20–30 nm were obtained (Fig. 2a). In contrast, GB exhibited Bi_2S_3 nanoparticles that are well anchored on the graphene sheets, which is in good agreement with the XRD data (Fig. 2b). This difference in the shape of Bi_2S_3 may be attributed to the interaction of bismuth ions with oxygen-containing

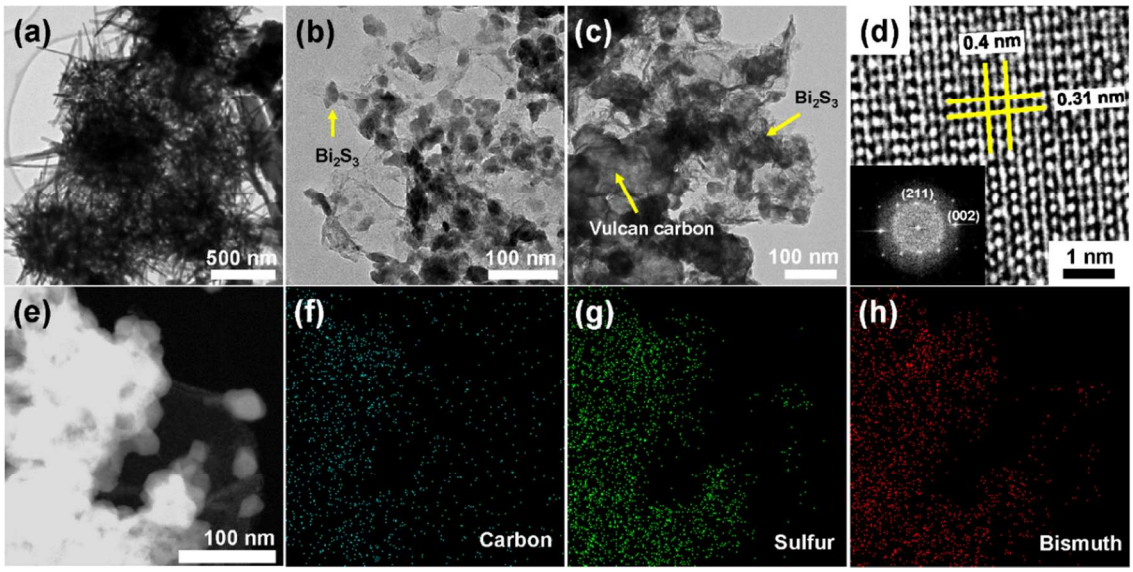

Fig. 3 TEM images of (a) Bi_2S_3 nanorods, (b) GB, and (c) GVB (3:1) nanocomposites; (d) HR-TEM image and FFT pattern of an individual Bi_2S_3 nanoparticle in GVB (3:1). The lattice spacing of 3.1 Å and 4 Å corresponds to the {211} and {001} plane of Bi_2S_3 (JCPDS no. 17-

0320), respectively. (e) Dark-field TEM image and (f, g, h) the corresponding C, S, and Bi element mapping.

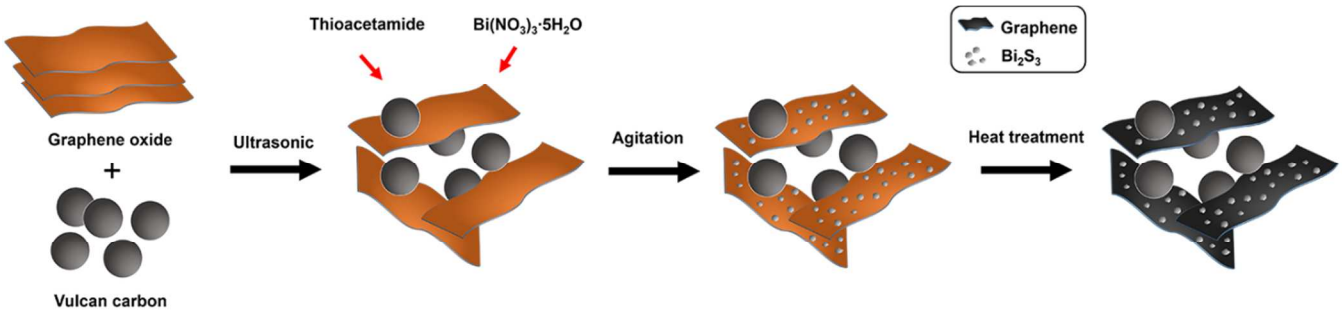

Fig. 4 Schematic illustration for the synthesis of 3D GVB nanocomposites

groups on the surface of GO. From the SEM images of all GVB samples, Vulcan carbons and Bi_2S_3 nanoparticles on graphene were clearly observed (Fig. 2c–g). The GVB samples show a rougher and crumpled surface, which is different from that of GB. This result indicates that when the Vulcan carbon was inserted into graphene sheets, it impedes the stacking of graphene sheets and enlarges the space between the graphene sheets effectively, leading to a crumpled and porous architecture. As shown in the SEM images of the GVB (1:1) and GVB (1:3) samples, excess Vulcan carbon is favorable for the formation of agglomerates, decreasing the exposure of graphene sheets. Therefore, only a certain quantity of Vulcan carbon can be used to form an ideal and uniform graphene–Vulcan carbon–Bi_2S_3 nanocomposite.

These structures and shapes were further characterized using TEM and high resolution TEM (HR-TEM), as shown in Fig. 3. At low magnification, we can clearly see that Bi_2S_3 nanorods agglomerated together into a sea-urchin shape of various diameters. Compared to GB, Vulcan carbons with diameters of 100–200 nm were observed in the GVB (3:1) sample, nevertheless, the physical properties of graphene and Bi_2S_3 nanoparticles (ex. size, shape and structure, et al.) are almost the same for both GB and GVB (3:1), suggesting that Vulcan carbons did not affect the formation of Bi_2S_3 nanoparticles (Fig. 3b and c). In a HR-TEM image of GVB (3:1), a Bi_2S_3 nanoparticle clearly shows 0.4 and 0.31 nm interplanar spacing, which correspond to the (001) and (211) plane, respectively, and has no stacking faults and dislocations, indicative of its highly single crystalline character. Fast Fourier Transform (FFT) patterns (inset of Fig. 3c) indicate the crystal planes of the orthorhombic Bi_2S_3 phase. Furthermore, EDX scanning elemental mapping of C, S, and Bi was performed to obtain the spatial distributions of the elemental content across the GVB (3:1). A similar coexistence of C, S, and Bi elements is observed on the entire Bi_2S_3 coating on Vulcan and graphene.

On the basis of the structural observations obtained from the above SEM and TEM images, the overall synthetic procedures of GVB are illustrated in Fig. 4. Vulcan carbon, a widely used commercial carbon supporting material, can be well dispersed in DI water, and the individual Vulcan carbons are adsorbed onto the surface of GO because of the π-π interactions. This three-dimensional carbon structure might be expected to increase the available surface area for deposition of Bi_2S_3 particles. TAA and bismuth nitride were added into the GO/Vulcan carbon hybrid solution to form a Bi_2S_3 nanoparticles through deposition of the metal ions onto the surface of carbon materials. After agitation by sonic treatment, small Bi_2S_3 particles are formed, and finally through the heating process GO is reduced to a conductive graphene sheet and the crystallinity of Bi_2S_3 nanoparticles is improved. During this process, Vulcan carbons on graphene prohibit the restacking between graphene sheets resulting from steric hindrance, leaving mesopores in the 3D hybrid structure. This unique structure provides advantages for the electrochemical performance in LIBs by forming an effective conducting network and pathways for lithium ion diffusion.

The porous structure and Brunauer–Emmett–Teller (BET) specific surface area of bare Bi_2S_3 nanorods, GB, and GVB nanocomposites were investigated by nitrogen isothermal adsorption. As shown in Fig. 5a and b, all products, except Bi_2S_3 nanorods, exhibit typical IV isotherm curves with hysteresis, corresponding to the existence of mesopores.[28] The specific surface area and the pore volume of Bi_2S_3 nanorods are greatly increased after the incorporation of graphene sheets, from 25.3 to 101.7 $m^2 g^{-1}$ and from 0.11 to 0.47 $cm^3 g^{-1}$, respectively. Interestingly, the GVB (3:1) nanocomposite shows higher specific surface area (114.6 $m^2 g^{-1}$) and larger pore volume (0.55 $cm^3 g^{-1}$) than that of GB, which could be attributed to the Vulcan carbon effectively inhibiting the restacking of graphene sheets to increase the interlayer spacing. On the other hand, with increasing Vulcan carbon content in the composites, the surface area gradually decreased to 74.1 [GVB (1:1)] and 43.36 $m^2 g^{-1}$ [GVB (1:3)] because of the relatively low surface area of Vulcan carbon (Fig. 5b and Table 1).

The expanded interlayer spacing between graphene layers was also confirmed by the Barrett−Joyner−Halenda (BJH) pore size distribution data. The GB sample shows that a majority of the pores lie between 10 and 100 nm, while most pores of the GVB (3:1) sample have a larger diameter range of 30–180 nm, suggesting that the basal spacing of graphene sheets is expanded by the Vulcan carbon spacer. The relatively large surface area of GVB nanocomposites would

Table 1 BET surface area and pore volume of Bi_2S_3, GV, and Bi_2S_3–graphene–Vulcan carbon nanocomposites

Sample	S_{BET} (m^2 g^{-1})	Pore volume (cm^3 g^{-1})
Bi_2S_3	25.3	0.11
GB	101.7	0.47
GVB (3:1)	114.6	0.55
GVB (1:1)	74.1	0.36
GVB (1:3)	43.36	0.35

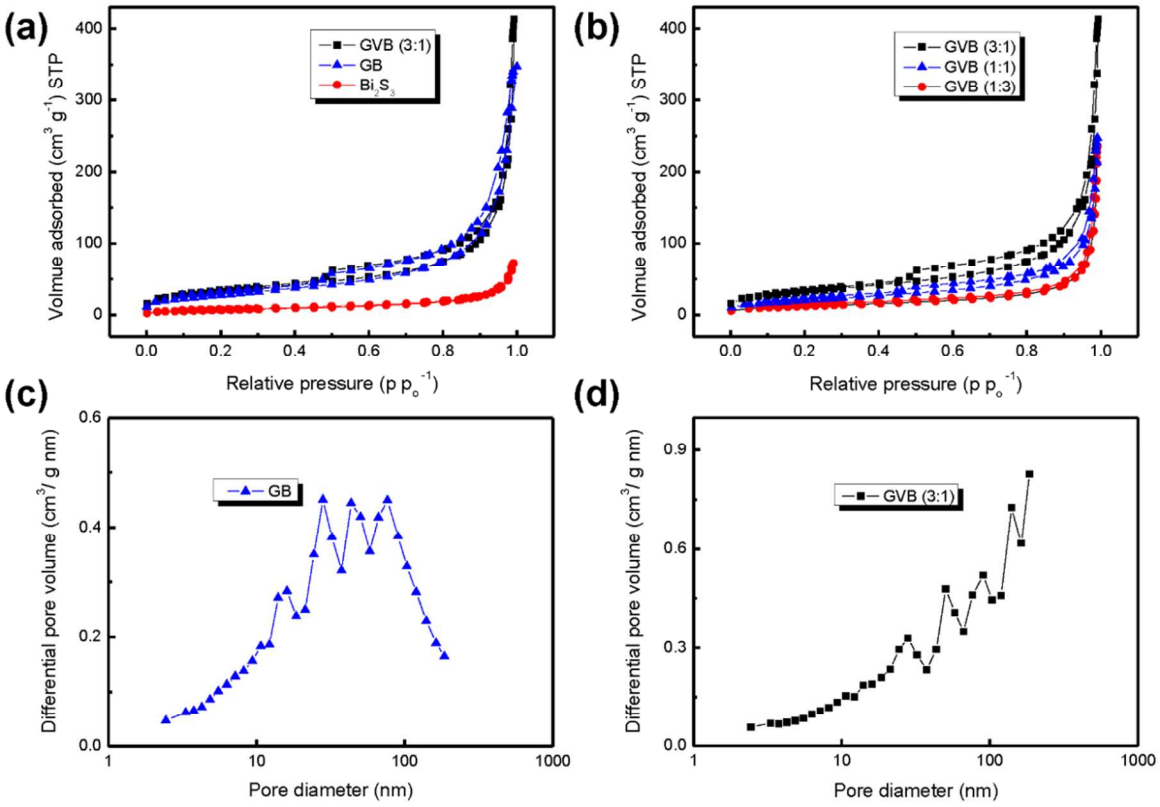

Fig. 5 N_2 adsorption-desorption isotherm curves of (a) bare Bi_2S_3, GB and GVB (3:1), and (b) GVB nanocomposites with different graphene/Vulcan carbon weight ratios. (c, d) BJH pore size distributions of GB and GVB (3:1), respectively.

provide more open channels to increase the electrolyte/electrode contact area, leading to high specific capacity and rate performance in LIBs.

The electrochemical performance of GVB (3:1) was examined by cyclic voltammetry (CV) and galvanostatic test. Fig. 6a shows the CV curves of the GVB (3:1) for the three initial cycles between 0.01 and 3.0 V at a scan rate of 0.1 mV s^{-1}. Over this potential range, the reaction mechanism between Bi_2S_3 and Li can be expressed by the following equation:[14, 29]

$$Bi_2S_3 + 12Li^+ + 12e^- \leftrightarrow 3Li_2S + 2Li_3Bi$$

In the first cathodic scanning, the peak centered at 1.5 V is ascribed to the Bi_2S_3 conversion to metallic Bi and Li_2S (Bi_2S_3 + $6Li^+ \leftrightarrow 2Bi + 3Li_2S$), while the peak at 0.5 V is attributed to the formation of the Li_3Bi alloy ($Bi + 3Li \leftrightarrow 2Li_3Bi$). Upon charging, the sharp peak that appears at 0.98 V is because of the Li_3Bi dealloying to metallic Bi, and the recovery of Bi_2S_3 occurred at 2.12 V. The anodic peak at 2.12 V is weaker than the 1.5 V cathodic peak, suggesting that partial Bi_2S_3 nanoparticles cannot be recovered. From the second cycle onwards, the CV graphs do not change positions or intensities of any of the peaks, indicating a favorable reversibility of the GVB.

Over the voltage window of 0.01–3.0 V, GVB was galvanostatically charged/discharged at a current density of 100 mA g^{-1}. The first charge/discharge process delivered a specific discharge capacity of 1219 mA h g^{-1} and a charge capacity of 745.6 mA h g^{-1} with an initial Coulombic efficiency of 61% (Fig. 6b). In the first discharge curve, two weak shoulders were observed at about 1.46 V and 0.5 V, which are in accordance with the CV curve of GVB. The irreversible capacity is mainly caused by the formation of a solid electrolyte interphase (SEI) on the surface of the active materials, as well as partially deactivated products by conversion and alloying reactions.[14, 29] Despite the initial capacity loss, the curves after the 1st

cycle show no large change, suggesting that the GVB becomes stable and nearly reproducible.

To obtain the long-term stability of electrodes, bare Bi_2S_3, GB, and GVB were tested at 100 mA g^{-1} for 100 cycles (Fig. 6c). Compared to bare Bi_2S_3, the GB delivers a high specific capacity, approximately 520 mA h g^{-1}, after 100 cycles, suggesting that the graphene materials provide enhanced mechanical properties to prevent the pulverization of Bi_2S_3 nanoparticles and high electron transfer as reported before.[30-32] Interestingly, the GVB exhibits a higher specific capacity of 702 mA h g^{-1} compared to that of GB after 100 cycles This specific capacity value is even higher than the theoretical capacity of Bi_2S_3 (625 mA h g^{-1}), which indicates carbon materials have contribute the overall capacity of electrode. However, even considering this fact, the capacity value of GVB (3:1) is superior to that reported in previous studies using only graphene, CNT, and amorphous carbon (Table 2). This result clearly showed the influence of Vulcan carbon in the composites. The Vulcan carbon attached on the surface of graphene reduces the π-π interaction between graphene sheets through steric hindrance, prohibiting the restacking of graphene sheets. Accordingly,

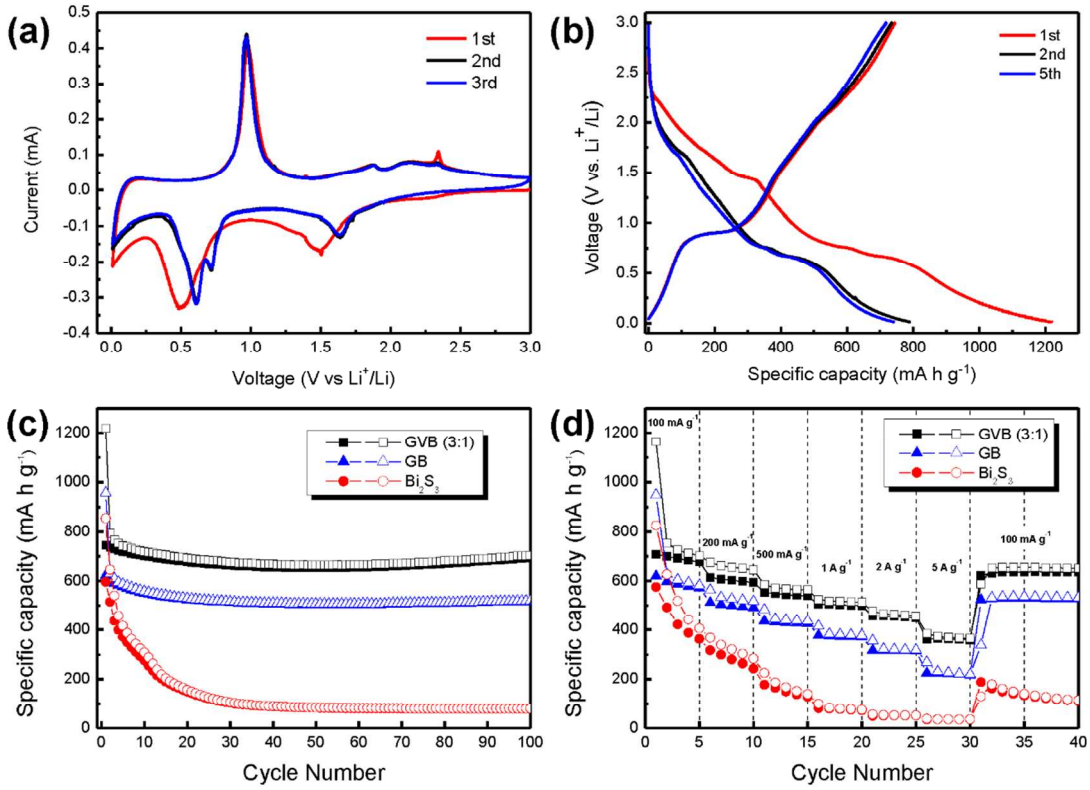

Fig. 6 (a) Cyclic voltammograms of GVB (3:1) nanocomposites at a scanning rate of 0.1 mV s^{-1}; (b) voltage profiles of GVB (3:1) nanocomposites and (c) comparative cycle performance of electrodes at a current density of 100 mA g^{-1}; (d) rate capability of GVB (3:1), GB, and Bi_2S_3 nanorods at different current densities.

graphene layers can maintain their large active contact area between the electrolyte and electrode, which produces enhanced lithium storage performance. Additionally, even though the GVB composites have relative low graphene contents compared to GB, they deliver higher specific capacity, suggesting that the improved the electrochemical properties are attributed to the unique 3D structure, not large carbon contents in composites.

Besides the superior and stable cycling, the GVB electrode also exhibits remarkable rate capability at various current densities. As shown in Fig. 6d, the GVB (3:1) delivers a capacity of 671 mA h g^{-1} at a charge-discharge rate of 0.5 A g^{-1}, and 614 mA h g^{-1} at 1 A g^{-1}. Even at very high rates of 2 and 5 A g^{-1}, it still shows high capacities of 561 and 471 mA h g^{-1}, respectively. More importantly, the discharge capacity of GVB increases back to 757 mA h g^{-1} as soon as the current density is reduced to 0.1 A g^{-1}. It seems that the Li-storage performance of the GVB is not deteriorated by high current density.

RSCPublishing

ARTICLE

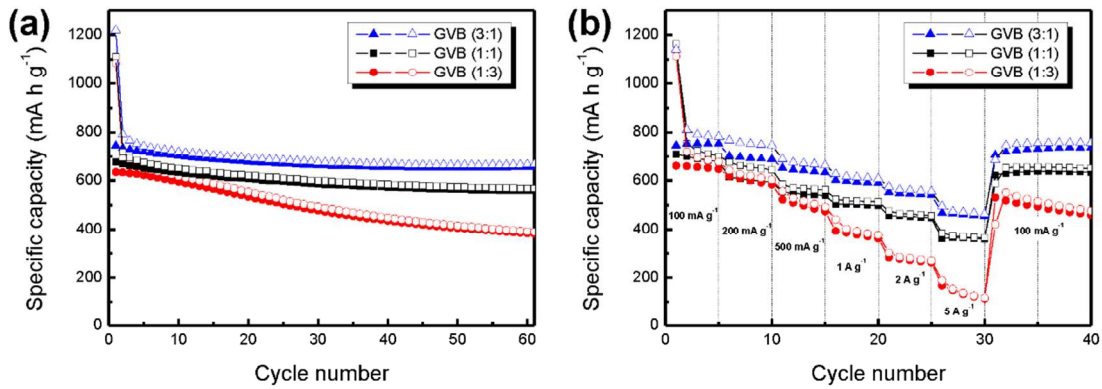

Fig. 7 (a) Comparative cycle performance of GVB nanocomposites with different graphene/Vulcan carbon weight ratios at a current density of 100 mA g^{-1}; (b) Rate properties of GVB nanocomposites at various current densities.

Table 2 Comparison of the specific discharge capacities of some related materials in the literature

Sample	Specific discharge capacity	Current density	Cycle	Reference
Graphene-Vulcan-Bi_2S_3 Nanocomposites	**702 mA h g^{-1}**	100 mA g^{-1}	100	Our work
Bi_2S_3 microspheres	74.7 mA h g^{-1}	100 mA g^{-1}	100	11
Carbon coated Bi_2S_3 nanomesh	472 mA h g^{-1}	120 mA g^{-1}	50	14
Graphene-Bi_2S_3 Nanocomposites	400.5 mA h g^{-1}	100 mA g^{-1}	50	15
Bi_2S_3-CNT hybrid	468 mA h g^{-1}	200 mA g^{-1}	100	29

To further investigate the effect of Vulcan carbon content in composites on electrochemical performance, GVB (1:1) and GVB (1:3) were evaluated at a current density of 100 mA g^{-1} for 60 cycles with GVB (3:1). From comparisons among the GVB samples, it was observed that the specific capacities of GVB nanocomposites gradually decreased with increasing Vulcan carbon content in the composites [GVB (3:1): 667, GVB (1:1): 569 and GVB (1:3): 390 mA h g^{-1}]. Even in case of the GVB (1:3) sample, its specific capacity value is lower than that of GB after 60 cycles (508 mA h g^{-1}). The trend is the same in the rate performance (Fig. 7b). These results could be attributed to the following factors. Firstly, the graphene nanosheets serve as a highly conductive substrate for rapid charge transfer, thus, a low graphene nanosheet content in composites increases the conductivity problem.[33, 34] Secondly, compared to Vulcan carbon, the graphene nanosheets have the advantage of reducing the mechanical stress in the electrode induced by the large volume variation of Bi_2S_3 nanoparticles upon lithiation and delithiation, resulting in the high electrode stability.[35, 36] Thirdly, introducing excess amount of Vulcan carbon leads to the formation of agglomerates, decreasing the surface area of the composites. Therefore, the overall electrochemical performance is decreased significantly. Finally, crumbled and porous structures of the GVB samples facilitate fast ion diffusion transfer and provide more open sites to increase the contact area with the electrolyte, leading to higher specific capacity value and rate performance in LIBs.

4. Conclusions

In summary, we have developed a facile sonochemical route to synthesize a 3D, structured Bi_2S_3–graphene–Vulcan carbon nanocomposite as an anode material for high-performance Li-ion batteries. The resulting Bi_2S_3–graphene–Vulcan carbon hybrid is composed of small Bi_2S_3 nanoparticles deposited well on graphene and Vulcan carbon. The intercalated Vulcan carbons are attached on the graphene to form very conductive 3D networks, which can act as a highly conductive substrate that is advantageous for high rate capabilities. Furthermore, the Vulcan carbons serve as a physical nanospacer to prevent the restacking of the graphene sheets, providing a large surface area of composites. As a result, the 3D Bi_2S_3–graphene–Vulcan carbon hybrids have more reaction sites and lower kinetic energy barrier for lithium ion insertion/deinsertion. Owing to these unique properties, the 3D hybrid material (graphene/Vulcan = 3:1 wt%) delivers a high capacity of 702 mA h g^{-1} and 471 mA h g^{-1} at current densities of 100 mA g^{-1} and 5 A g^{-1}, respectively, which are higher than that of bare Bi_2S_3 nanorods and Bi_2S_3–graphene hybrids. It is believed that such graphene/Vulcan carbon-based hybrid materials will be useful in energy storage systems and other important applications.

Acknowledgements

This work was supported by a grant from the Ministry of Science, ICT and Future Planning, Republic of Korea (2014034504) and by the Center for Integrated Smart Sensors funded by the Ministry of Science, ICT and Future Planning, Republic of Korea, as Global Frontier Project (CISS-012M3A6A6054186).

Notes and references

[a]Program in Nano Science and Technology, Graduate School of Convergence Science and Technology, Seoul National University, 145 Gwanggyo-ro, Yeongtong-gu, Suwon–si, Gyeonggi-do, 443-270, Republic of Korea.

Fax: +82-31-8889148; Tel: +82-31-8889141; E-mail: parkat9@snu.ac.kr

[b]Advanced Institutes of Convergence Technology, 145 Gwanggyo-ro, Yeongtong-gu, Suwon–si, Gyeonggi-do, 443-270, Republic of Korea.

[c]Department of Chemistry, Seoul National University, Seoul 151-747, Republic of Korea.

1 J. A. Jiang, Y. Y. Li, J. P. Liu and X. T. Huang, *Nanoscale*, 2011, **3**, 45.
2 W. J. Zhang, *J. Power Sources*, 2011, **196**, 13.
3 B. Jang, O. B. Chae, S. K. Park, J. Ha, S. M. Oh, H. B. Na and Y. Piao, *J. Mater. Chem. A*, 2013, **1**, 15442.
4 H. S. Kim, Y. Piao, S. H. Kang, T. Hyeon and Y. E. Sung, *Electrochem. Commun.*, 2010, **12**, 382.
5 S. K. Park, A. Jin, S. H. Yu, J. Ha, B. Jang, S. Bong, S. Woo, Y. E. Sung and Y. Piao, *Electrochim. Acta*, 2014, **120**, 452.
6 S. J. Ding and X. W. Lou, *Nanoscale*, 2011, **3**, 3586.
7 S. K. Park, S. H. Yu, S. Woo, B. Quan, D. C. Lee, M. K. Kim, Y. E. Sung and Y. Piao, *Dalton Trans.*, 2013, **42**, 2399.
8 B. Wu, H. H. Song, J. S. Zhou and X. H. Chen, *Chem. Commun.*, 2011, **47**, 8653.
9 S. K. Park, S. H. Yu, S. Woo, J. Ha, J. Shin, Y. E. Sung and Y. Piao, *CrystEngComm*, 2012, **14**, 8323.
10 H. Hwang, H. Kim and J. Cho, *Nano Lett.*, 2011, **11**, 4826.
11 Z. Zhang, C. K. Zhou, H. Lu, M. Jia, Y. Q. Lai and J. Li, *Mater. Lett.*, 2013, **91**, 100.
12 X. Feng, X. M. He, W. H. Pu, C. Y. Jiang and C. R. Wan, *Ionics*, 2007, **13**, 375.
13 Y. Zhao, T. T. Liu, H. Xia, L. Zhang, J. X. Jiang, M. Shen, J. F. Ni and L. J. Gao, *J. Mater. Chem. A*, 2014, **2**, 13854.
14 Y. Zhao, D. L. Gao, J. F. Ni, L. J. Gao, J. Yang and Y. Li, *Nano Res.*, 2014, **7**, 765.
15 Z. Zhang, C. K. Zhou, L. Huang, X. W. Wang, Y. H. Qu, Y. Q. Lai and J. Li, *Electrochim. Acta*, 2013, **114**, 88.
16 D. Li, M. B. Muller, S. Gilje, R. B. Kaner and G. G. Wallace, *Nat. Nanotechnol.*, 2008, **3**, 101.
17 S. B. Yang, X. L. Feng, L. Wang, K. Tang, J. Maier and K. Mullen, *Angew. Chem. Int. Ed.*, 2010, **49**, 4795.
18 S. Woo, J. Lee, S. K. Park, H. Kim, T. D. Chung and Y. Piao, *J. Power Sources*, 2013, **222**, 261.
19 S. Woo, Y. R. Kim, T. D. Chung, Y. Piao and H. Kim, *Electrochim. Acta*, 2012, **59**, 509.
20 S. Q. Chen, P. Chen and Y. Wang, *Nanoscale*, 2011, **3**, 4323.
21 J. Shin, K. Park, W. H. Ryu, J. W. Jung and I. D. Kim, *Nanoscale*, 2014, **6**, 12718.
22 Y. S. Kim, K. Kumar, F. T. Fisher and E. H. Yang, *Nanotechnology*, 2012, **23**, 015301.
23 Q. Cheng, J. Tang, J. Ma, H. Zhang, N. Shinya and L. C. Qin, *Phys. Chem. Chem. Phys.*, 2011, **13**, 17615.
24 D. S. Zhang, X. R. Wen, L. Y. Shi, T. T. Yan and J. P. Zhang, *Nanoscale*, 2012, **4**, 5440.
25 Y. Fang, Y. Y. Lv, R. C. Che, H. Y. Wu, X. H. Zhang, D. Gu, G. F. Zheng and D. Y. Zhao, *J. Am. Chem. Soc.*, 2013, **135**, 1524.
26 D. C. Marcano, D. V. Kosynkin, J. M. Berlin, A. Sinitskii, Z. Z. Sun, A. Slesarev, L. B. Alemany, W. Lu and J. M. Tour, *ACS Nano*, 2010, **4**, 4806.
27 S. S. Warule, N. S. Chaudhari, B. B. Kale, S. Pandiraj, R. T. Khare and M. A. More, *CrystEngComm*, 2013, **15**, 890.
28 L. F. Shen, X. G. Zhang, H. S. Li, C. Z. Yuan and G. Z. Cao, *J. Phys. Chem. Lett.*, 2011, **2**, 3096.
29 J. F. Ni, Y. Zhao, T. T. Liu, H. H. Zheng, L. J. Gao, C. L. Yan and L. Li, *Adv. Energy Mater.*, 2014, **4**, 1400798.
30 S. K. Park, S. H. Yu, N. Pinna, S. Woo, B. Jang, Y. H. Chung, Y. H. Cho, Y. E. Sung and Y. Piao, *J. Mater. Chem.*, 2012, **22**, 2520.
31 Z. S. Wu, W. C. Ren, L. Wen, L. B. Gao, J. P. Zhao, Z. P. Chen, G. M. Zhou, F. Li and H. M. Cheng, *ACS Nano*, 2010, **4**, 3187.
32 G. M. Zhou, D. W. Wang, F. Li, L. L. Zhang, N. Li, Z. S. Wu, L. Wen, G. Q. Lu and H. M. Cheng, *Chem. Mater.*, 2010, **22**, 5306.
33 J. X. Zhu, T. Zhu, X. Z. Zhou, Y. Y. Zhang, X. W. Lou, X. D. Chen, H. Zhang, H. H. Hng and Q. Y. Yan, *Nanoscale*, 2011, **3**, 1084.
34 Y. Q. Luo, S. S. Fan, N. Y. Hao, S. L. Zhong and W. C. Liu, *Dalton Trans.*, 2014, **43**, 15317.
35 M. P. Yu, A. J. Wang, Y. S. Wang, C. Li and G. Q. Shi, *Nanoscale*, 2014, **6**, 11419.
36 D. B. Kong, H. Y. He, Q. Song, B. Wang, W. Lv, Q. H. Yang and L. J. Zhi, *Energy Environ. Sci.*, 2014, **7**, 3320.

